Chemical sputtering by H_2^+ and H_3^+ ions during silicon deposition

Chemical sputtering by H_2^+ and H_3^+ ions during silicon deposition

K. Landheer, W. J. Goedheer, I. Poulios, R. E. I. Schropp, and J. K. Rath

Citation: Journal of Applied Physics **120**, 053304 (2016); doi: 10.1063/1.4960351
View online: http://dx.doi.org/10.1063/1.4960351
View Table of Contents: http://aip.scitation.org/toc/jap/120/5
Published by the American Institute of Physics

Chemical sputtering by H_2^+ and H_3^+ ions during silicon deposition

K. Landheer,[1,a)] W. J. Goedheer,[2] I. Poulios,[1] R. E. I. Schropp,[3] and J. K. Rath[1]
[1]*Debye Institute for Nanomaterials Science-Physics of Devices, Utrecht University, 5656 AE Eindhoven, The Netherlands*
[2]*FOM Institute DIFFER-Dutch Institute for Fundamental Energy Research, 5600 HH Eindhoven, The Netherlands*
[3]*Department of Applied Physics, Plasma and Materials Processing, Eindhoven University of Technology, 5600 MB Eindhoven, The Netherlands*

(Received 14 March 2016; accepted 22 July 2016; published online 5 August 2016)

We investigated chemical sputtering of silicon films by H_y^+ ions (with y being 2 and 3) in an asymmetric VHF Plasma Enhanced Chemical Vapor Deposition (PECVD) discharge in detail. In experiments with discharges created with pure H_2 inlet flows, we observed that more Si was etched from the powered than from the grounded electrode, and this resulted in a net deposition on the grounded electrode. With experimental input data from a power density series of discharges with pure H_2 inlet flows, we were able to model this process with a chemical sputtering mechanism. The obtained chemical sputtering yields were (0.3–0.4) ± 0.1 Si atom per bombarding H_y^+ ion at the grounded electrode and at the powered electrode the yield ranged from (0.4 to 0.65) ± 0.1. Subsequently, we investigated the role of chemical sputtering during PECVD deposition with a series of silane fractions S_F ($S_F(\%) = [SiH_4]/[H_2]*100$) ranging from $S_F = 0\%$ to 20%. We experimentally observed that the SiH_y^+ flux is not proportional to S_F but decreasing from $S_F = 3.4\%$ to 20%. This counterintuitive SiH_y^+ flux trend was partly explained by an increasing chemical sputtering rate with decreasing S_F and partly by the reaction between H_3^+ and SiH_4 that forms SiH_3^+. *Published by AIP Publishing.* [http://dx.doi.org/10.1063/1.4960351]

I. INTRODUCTION

Hydrogenated micro-crystalline silicon (μc-Si:H) and amorphous silicon (a-Si:H) layers are used in solar cells and are usually created by capacitively coupled Plasma Enhanced Chemical Vapor Deposition (cc PECVD). In a cc PECVD plasma, ions are formed that bombard the growing layer of the Si material. It is well known that ion bombardment from SiH_4-H_2 PECVD discharges affects the bonding structure within the silicon network,[1,2] compactness,[3] uniformity, degree of hydrogenation[4] of the layer, and its interface with the substrate.[1] But chemical sputtering of Si by H_2^+ and H_3^+ (i.e., H_y^+) ions in a PECVD discharge has not been analyzed in detail before.

In an earlier publication,[5] we observed a counterintuitive trend: the SiH_y^+ flux was not proportional to the silane fraction (S_F) in the feedstock gas mixture. We also observed that for S_F from 1.7% to 20%, the H_y^+ flux falls significantly and at low S_F the H_y^+ bombardment deposits a large amount of energy per deposited Si atom (e.g., 29 eV at $S_F = 1.7\%$). Moreover, we measured a significant SiH_3^+ flux at $S_F = 0\%$.

In an effort to reveal possible causes for the SiH_y^+ flux trend, we hypothesized that etching through chemical sputtering by H_y^+ bombardment creates etch products that contribute to the SiH_y^+ flux at low S_F. We are not the first to attribute a role to hydrogenic (H_y^+) ions in the etching process. Leroy *et al.*[6] measured and modeled rf PECVD under similar deposition conditions (40 Pa and $S_F = 11\%$) and suggested that etching during deposition was mainly by H_y^+ ions, since the contribution of atomic hydrogen (H) etching as expected by the model of Abrefah and Olander[7] was negligible (<3%). However, their analysis focused on radicals in the discharge and not on ion bombardment. In this study, we compare experimental data with results from a 2D fluid model and a Monte Carlo model to develop a chemical sputtering model for PECVD discharges as well as to reach an understanding of the counterintuitive SiH_y^+ flux trend.

For a chemical sputtering process, the ions must be able to penetrate into the target material with a collision cascade and create strained Si–Si bonds in the film network. The minimal ion energy (E_{dam}) needed for these processes is about 20 eV for H_y^+ ions that are implanted in crystalline Si (c-Si).[9] The H_3^+ ion is the main component of the H_y^+ flux in our PECVD plasmas. The H_3^+ ion converts into either molecular and atomic hydrogen (H_2 + H) or only atomic hydrogen (3 H) by dissociative recombination at the moment of impact.[11] Desorbing species are also formed near the ion penetration depth and this shows the chemical activity of the hydrogenic ions.[10] Atomic H diffusing through Si can break a weak Si–Si bond, it can passivate the Si dangling bonds formed, and it can recombine with another H atom and form molecular H_2. Si–Si bond breaking reactions involved in atomic H etching have an activation energy of about 0.4 eV.[12] However, Wanka and Schubert[13] observed that the a-Si:H etch rate by atomic H, formed with a hot-tungsten filament, reduces for temperatures above room temperature. Two mechanisms can explain this observation: reduced atomic H surface coverage at elevated temperatures due to either enhanced atomic H recombination and desorption[14] or enhanced atomic H diffusion into the bulk.[7] The chemical

a)Author to whom correspondence should be addressed. Electronic mail: c.landheer@uu.nl.

sputtering rate of H_y^+ ions is relatively constant from room temperature to 130 °C (Refs. 15 and 16) and this suggests that the atomic H surface coverage is not rate limiting for the chemical sputtering process in this temperature range. Physical ion sputtering of Si can be excluded because the ion bombardment energies in our SiH_4-H_2 VHF PECVD discharges remain below the threshold energy for physical sputtering. This threshold energy depends on the mass ratio of projectile and target atom and is about 50 eV for Ar^+ ions[8] that sputter Si. Therefore, it is not momentum transfer that removes etch products from the surface in the chemical sputtering process but thermal desorption.

It is important to realize that the chemical sputtering on both electrodes can be different. The process in which silicon is etched from the powered electrode and redeposited on the grounded electrode is known as chemical transport.[17] In this process, the etch rate is lower than the gross deposition rate at the grounded electrode and at the powered electrode the etch rate is higher than the deposition rate. The net deposition rate on the grounded electrode can have several reasons, among others: a difference in the H_y^+ ion flux between the powered and grounded electrode, a difference in temperature, and an ion energy dependent etch yield.

Recent theoretical studies by Heil *et al.*[18] and Lafleur *et al.*[19] have shown how an Electrical Asymmetry Effect (EAE) can be created in a geometrically symmetric reactor with a tailored waveform. This method is applied by Bruneau *et al.*[20] for the deposition of Si at low S_F. In this study, we aim to further increase the understanding of the capacitive discharges at low S_F that are excited with a single sinusoidal wave and this is also relevant for excitation by complex waveforms, as used for the EAE method. In this study, we used a reactor design similar to the GEC reference reactor.[21] The deposition conditions used are in the regime of good quality a-Si:H as was confirmed by tests[22] using the material created with $S_F = 1.7\%$ as the passivation layer in flat silicon heterojunction (SHJ) solar cells.

II. EXPERIMENTAL

The parallel plate reactor and the plasma diagnostics used in the experiments are depicted in Fig. 1. The dimensions of our pillbox reactor are as follows: the radius of the powered electrode is 7.85 cm, the radius of the substrate electrode is 8.5 cm, and the separation between the electrodes is 2.7 cm. In between the powered electrode rim and the inner rim of the grounded guarding shield, a ceramic ring is present with a width of 1 cm. The rim of the grounded guarding shield is in contact with the wall of the reactor. The diameter of the reactor is 20 cm.

In order to test the chemical sputtering model in our VHF PECVD reactor and to determine the etch yield Y (number of Si atoms etched per impinging H_y^+ ion), we performed two series of Si depositions on glass. We applied a pure H_2 plasma at power densities of 57, 114, and 171 mW cm^{-2} in a reactor with Si on the electrodes and walls. This resulted in Si deposition on a strip of Corning glass substrate, mounted on the grounded electrode. The H_2 gas flow in these experiments was 60 sccm at 25 Pa. In the first series, the substrate temperature was 130 °C and in the second series the complete reactor was cooled down to room temperature.

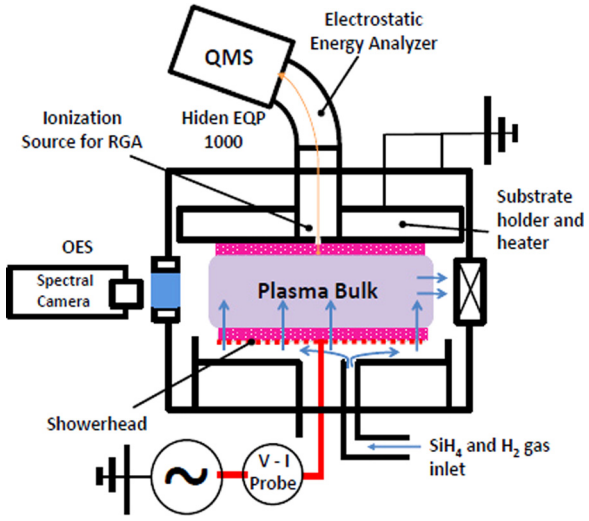

FIG. 1. Schematic diagram of the cylindrical parallel plate reactor with a Hiden EQP plasma analyzer (for IMS and RGA measurements), OES spectrometer, and V-I probe. The reactor dimensions are not to scale.

The Si layers deposited on the glass on the grounded electrode were a-Si:H layers thinner than 100 nm. The Si layers on the powered electrode are directly deposited on the stainless steel showerhead electrode. Their crystallinity and hydrogenation are not monitored *in situ* and therefore unknown. The chemical sputtering etch yield depends on the crystallinity of the material, which is not taken into account in our chemical sputtering model. The Si layers on the powered electrode are most probably amorphous near the surface due to the intense ion bombardment.

The silane fraction series from $S_F = 0\%$ to 20% had the following plasma conditions: a gas pressure (p) of 25 Pa, a power density (P_{rf}) of 57 mW cm^{-2}, and a substrate temperature (T_s) of 130 °C. At $S_F = 20\%$, gas flows of 10 sccm SiH_4 and 50 sccm H_2 were used. We subsequently decreased S_F in our experiment by keeping the total flow at 60 sccm and reducing the SiH_4 flow in steps to 0 sccm. During processing, the gas pressure in the reactor was monitored with a Baratron pressure gauge and was maintained constant with a throttle valve between the reactor and pumps. The mass spectrometer is separately pumped and its pressure was kept below 5×10^{-4} Pa.

The Ion Energy Distributions (IEDs) of H_2^+, H_3^+, SiH_2^+, SiH_3^+, $Si_2H_4^+$, and $Si_2H_5^+$ in the S_F series were measured with a plasma analyzer. Fluid model and IED simulations were performed for the same ions, although in the simulation SiH_2^+, SiH_3^+, plus very small amounts of SiH^+ and Si^+ were put in a lump sum labelled SiH_y^+. The $Si_2H_y^+$ (with y = 0–5) ions were put in the lump sum $Si_2H_y^+$. In Section V, we model different reaction mechanisms for SiH_2^+ and SiH_3^+ and look at their contribution to the total SiH_y^+ flux at low S_F.

The IED of a selected atomic mass unit (only singly ionized ions are expected) was measured by scanning an energy range with the Electrostatic Energy Analyzer (EEA) and

keeping the quadrupole mass spectrometer (QMS) of the plasma analyzer steady at the selected mass. The energy resolution (FWHM) of the EEA is 2.55 eV and independent of the kinetic energy measured. Only ions that enter the plasma analyzer with an angle of incidence less than 15° are analyzed by the EEA. We label this measurement mode Ion Mass Spectrometry (IMS). Electrons are repelled and positive ions are attracted to the inlet of the plasma analyzer by the negative extractor voltage (−10 V) in IMS measurements. Before every measurement series, we optimized all lenses of the plasma analyzer for maximum transmission at 40 amu with an Ar plasma. Since the IEDs of the complete S_F series are measured with constant transmission settings, the flux of the selected ion species can be compared between different S_F. We measured a total ion flux of the order of 10^{19} ions m^{-2} s^{-1} with a retarding field energy analyzer for discharges with the same plasma conditions in an identical reactor.[23] Our simulation results show the same order of magnitude for the total ion flux.

Near its orifice, the plasma analyzer has an ionization section to ionize neutrals and radicals with a mono-energetic electron beam. This device is active in the Residual Gas Analysis (RGA) measurement mode. Neutrals from the plasma can be measured in RGA mode: in this case, the ions from the plasma are repelled by a positive voltage of +60 V on the extractor. We verified in the IMS mode that no signal is detected when the extractor voltage is kept at +60 V. The silane depletion fraction F_D is the fraction of SiH_4 that is consumed in plasma reactions.[24] The measured F_D is determined with RGA measurements and is the ratio of the loss in SiH_2^+ intensity as a consequence of switching on the plasma to the SiH_2^+ intensity without the plasma (i.e., in the presence of the gas mixture). Simultaneously, we measure the UV/VIS-light spectrum coming from the plasma halfway between the powered and grounded electrodes and monitor the power coupled into the discharge with a current-voltage (V–I) probe. The light spectrum is used to determine the Si*(288 nm) Optical Emission Spectroscopy (OES) peak intensity.

III. SIMULATIONS

A. Fluid model

We compared our experimental results with the modeling results of a self-consistent fluid model of the SiH_4-H_2 discharge. The 2-dimensional model of the cylindrically symmetric reactor, with the spatial dimensions r and z, was built and described by Nienhuis *et al.*[25] In the analysis presented here, the fluid model is used to compute an extensive set of time varying plasma parameters in the discharge. The following parameters have been modelled: electric potential, electron energy distribution function, electron density, and radical and ion densities (both positive and negative ions) as well as their fluxes to the electrodes. These quantities and distributions are used to explain the experimental ion bombardment trends and are used to calculate the Si* OES line intensity.[26,27]

The fluid model[25] simulates a-Si:H layer growth with a surface reaction probability β and sticking coefficient s. For example, β is 0.26 and s is 0.09 for SiH_3. For Si_xH_{2x+1} ($x > 1$) radicals, the same β and s are assumed. For SiH_2 on the other hand β is 1 and s is 0.7. All $Si_xH_y^+$ ions bombarding the surface are assumed to contribute to the simulated deposition rate. This will result in an upper limit for the deposition rate as not all $Si_xH_y^+$ ions stick to the surface; some ions may, for example, strip atomic H from a Si-H bond on the surface. The a-Si:H deposition rate is determined by dividing the number of deposited Si atoms by the Si atom density, being $5 \times 10^{28}\,m^{-3}$ ($=5 \times 10^{19}\,m^{-2}\,nm^{-1}$). Incident atomic H from the plasma abstracts a bonded H atom from the surface with a probability of 0.8 and subsequently desorbs as H_2. The chance that an incident H atom reflects is 0.2. In the simulations, the hydrogen content of the Si films is maintained at 10 at. % by adjusting the desorption of H_2.

The fluid model has restrictions in its applicability. It simulates collision-dominated PECVD discharges and therefore the gas pressure should be above 10 Pa. In the fluid model,[24] the substrate temperature has only an effect on the gas density. The (surface) temperature is not influenced by the plasma or chemical reactions on the surface.

The model of Nienhuis *et al.*[25] was extended in this research with hydrogen chemistry, such as the production of H_3^+ ($H_2^+ + H_2 \rightarrow H_3^+ + H$).[28] Also electron energy dissipation processes have been added, among others the process $H_2 + e^- \rightarrow H_{2,\alpha}^* \rightarrow 2\,H + e^-$ with radiative relaxation, that creates visible light emission from the plasma.[29] However, etching or chemical sputtering was not included in the model, as this would require as yet unavailable data.

B. Monte Carlo model

A Monte Carlo model based on the null collision method[30] is used to simulate the distribution of bombardment energies of H_2^+, H_3^+, SiH_y^+, and $Si_2H_y^+$ ions on the electrodes. To simulate ion trajectories through the reactor, the Monte Carlo model uses the space and time dependent electric field and ion production, generated by the fluid model. Ions are released one at a time. The release time (t_0) and position (z_0) on the axis of the reactor ($r = 0$) are determined by a randomized drawing from the ion production distribution, S(t, z), during one full rf period. After release, the ion can be accelerated by the electric field and it can collide with a neutral of the feedstock gas (SiH_4 or H_2). The time step used to advance the ions between collisions is taken equal to the time step in the fluid simulation, 1/256 of the rf period (6.5×10^{-11} s). A collision between two reactants can result in the following type of interactions: resonant charge exchange reactions,[28,31] elastic collisions (using the hard sphere model, as recommended by Perrin *et al.*[32]), and the production of different ion species. The ion continues its trajectory until it hits another neutral or one of the electrodes. At the moment the ion hits one of the electrodes, the impact energies and angles are recorded.

Simulated IEDs count only ions that impinge on the substrate surface at an incident angle less than 15°, in agreement with experimental conditions. However, all angles are considered in the computation of the ion flux and the ion energy

flux. For the IEDs at the powered electrode we rely on the model, because only the dc self-bias V_{DC} and the rf voltage amplitude (V_{rf}) are measured on the powered electrode. Since the kinetic energy of the ions in the sheath is higher than in the plasma bulk, reactions in the sheath can be endothermic and take place at a different rate than in the plasma bulk. For example, the dissociation of H_3^+ ($H_3^+ + H_2 \rightarrow H_2^+ + H_2 + H$)[28] takes place in the sheath but not in the plasma bulk. IED modeling results are shown in Section 2 of the supplementary material.

C. The modeling of chemical sputtering

Chemical sputtering experiments with discharges created with a pure H_2 inlet flow were performed to find the etch yield (Y) on the electrodes. We use the diagram of Fig. 2 to tag the different silane flows and hydrogen fluxes involved in the chemical sputtering model. In our experiments, a glass substrate is mounted on the grounded electrode and a Si layer is present on the powered electrode. The H_2 plasma etches Si from the powered electrode and this creates a flow $Si_{inlet,P}$[atoms s^{-1}] of Si_xH_{2x+2} neutrals into the discharge. Part of the desorbed neutrals are dissociated and ionized in the discharge and form the gross deposition rate on the grounded ($r_{gross,G}$[nm/h]) or powered electrode. Once Si deposits on the glass, it can also be etched away and this forms the flow $Si_{inlet,G}$[atoms s^{-1}]. The term $r_{net,G}$[nm/h] is the net Si deposition rate on the glass, which is experimentally determined from the Si layer thickness and H_2 plasma exposure time. The amount of SiH_4 and Si_2H_6 created by the chemical sputtering at $P_{rf} = 57$ mW cm^{-2} is quantified with the SiH_2^+ and $Si_2H_4^+$ RGA signals.

The 2D fluid model computes the gross deposition rate $r_{gross,G}$ (without etching) based on the amount of SiH_4 in the feedstock. Moreover, it computes the H_y^+ flux to the grounded ($\Gamma_{G,Hy+}$) and powered ($\Gamma_{P,Hy+}$) electrodes. The atomic H fluxes to the grounded ($G_{a,flux}$) and powered ($P_{a,flux}$) electrodes are also modeled and are used in the argumentation. Our chemical sputtering model is summarized in Equations (1) and (2) below and assumes that the Si etch rate is determined by the H_y^+ flux of ions with energies above 20 eV. The flow of Si atoms that are brought into the discharge by chemical sputtering on the grounded and powered electrodes can be calculated as follows:

$$Si_{inlet,G/P} = Y_{G/P}[\text{atoms/ion}]\Gamma_{G/P,Hy+}[\text{ions m}^{-2}\text{s}^{-1}]\, A_{G/P}[\text{m}^2], \quad (1a)$$

$$Si_{inlet}[\text{atoms s}^{-1}] = Si_{inlet,G}[\text{atoms s}^{-1}] + Si_{inlet,P}[\text{atoms s}^{-1}], \quad (1b)$$

where $Y_{G/P}$ is the yield, i.e., the number of Si atoms etched per impinging H_y^+ ion, on the grounded (Y_G) or powered (Y_P) electrode. A_G and A_P denote their area. Si_{inlet} is thus the amount of Si atoms per second that is brought into the discharge. In the model, we assume that all etched Si atoms enter the discharge as SiH_4, and Si_{inlet} is then converted to sccm SiH_4 and subsequently used to determine $r_{gross,G}$ with the fluid model. The net deposition rate $r_{net,G}$ on the glass substrate as a consequence of gross deposition ($r_{gross,G}$) and etching by chemical sputtering ($r_{etch,G}$[nm/h]) is modelled with the formulas

$$r_{etch,G}[\text{nm h}^{-1}] = \frac{3.6\times10^3[\text{s h}^{-1}]}{n_{Si}[\text{atoms m}^{-2}\text{nm}^{-1}]} \times Y_G[\text{atoms/ion}]\Gamma_{G,Hy+}[\text{ions m}^{-2}\text{s}^{-1}], \quad (2a)$$

$$r_{net,G}[\text{nm h}^{-1}] = r_{gross,G}[\text{nm h}^{-1}] - r_{etch,G}[\text{nm h}^{-1}], \quad (2b)$$

where n_{Si} is the Si atomic density of pure silicon, being $5\times10^{19}\,\text{m}^{-2}\,\text{nm}^{-1}$, and 3.6×10^3 s h^{-1} converts per second into per hour. $r_{gross,G}$ is calculated by the fluid model based on the equivalent SiH_4 inlet flow. Combining measured and computed quantities for two P_{rf} settings gives sufficient information to obtain the values of Y_G and Y_P. The starting point is the discharge at a power of 57 mW cm^{-2}, where we have additional information on the silane inflow from the RGA measurements.

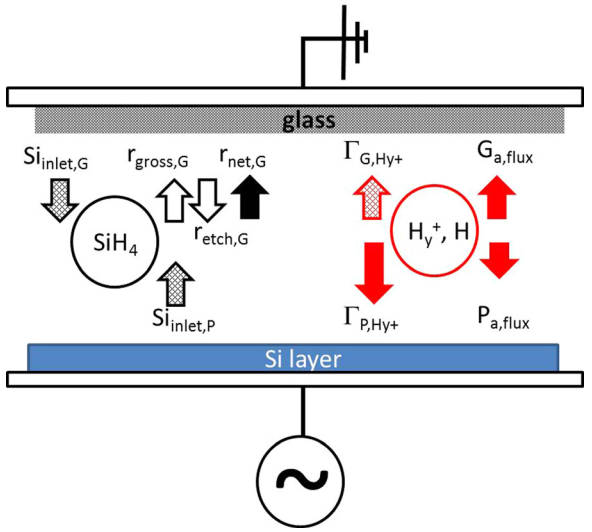

FIG. 2. Diagram of the parallel plate reactor with on the left side the silane flows ($Si_{inlet,G}$ and $Si_{inlet,P}$) and the deposition ($r_{gross,G}$ and $r_{net,G}$) and etch ($r_{etch,G}$) rates and on the right side the H_y^+ ion ($\Gamma_{G,Hy+}$ and $\Gamma_{P,Hy+}$) and atomic H fluxes ($G_{a,flux}$ and $P_{a,flux}$). $r_{net,G}$ can be quantified by depositions on glass, the other flows and fluxes are determined by simulations.

IV. RESULTS

A. The chemical sputtering yield

In order to provide the chemical sputtering model with input data, we performed PECVD Si depositions on a glass substrate with only H_2 feedstock gas. We made series of Si depositions both at $T_s = 130\,^\circ$C and at $T_s = 25\,^\circ$C at three different P_{rf}. Table I shows $r_{net,G}$ of the two series. At $P_{rf} = 57$ mW cm^{-2}, nothing was deposited on the glass. Therefore, we started the experiment with a 40 nm thick a-Si:H layer on glass to see if the layer is etched. The P_{rf} series at $T_s = 25\,^\circ$C shows only a slightly lower $r_{net,G}$ than at $T_s = 130\,^\circ$C for $P_{rf} = 114$ and 171 mW cm^{-2}.

For the computation of the etch yields Y_G and Y_P at $T_s = 130\,^\circ$C, we used three assumptions: Y_G does not change in our P_{rf} series since the H_y^+ ion energies do not increase a

TABLE I. Experimental results for H_2 plasma etching at 25 Pa.

P_{rf} (mW cm^{-2})	$r_{net,G}$ $T_s = 130\,°C$ (nm/h)	$r_{net,G}$ $T_s = 25\,°C$ (nm/h)
57	−30[a]	0[a]
114	+95	+70
171	+137	+132

[a]Determined by starting with a 40 nm thick a-Si:H layer on glass. Due to the H_2 plasma treatment the a-Si:H layer may become more crystalline.

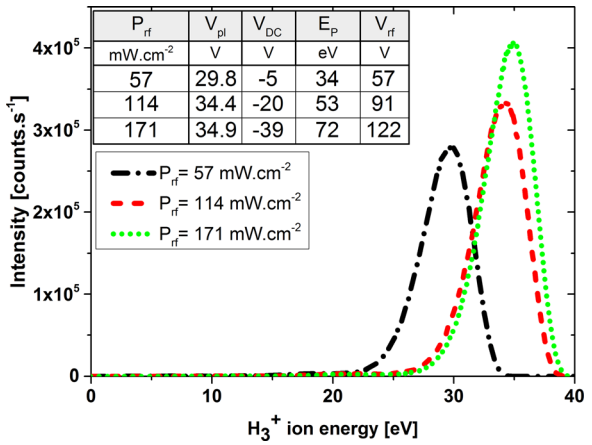

FIG. 3. The H_3^+ IEDs on the grounded electrode as measured with IMS. The P_{rf} series at $T_s = 130\,°C$ is shown. The flow is 60 sccm H_2 and the pressure is 25 Pa. The inset table shows how V_{pl}, V_{DC}, Ep, and V_{rf} increase with P_{rf}.

lot (see Fig. 3), Y_P can increase for higher H_y^+ bombardment energies, and $r_{gross,G}$ is proportional to the SiH_4 inlet flow. In Fig. 3, the measured H_3^+ IEDs of the P_{rf} series created with only H_2 feedstock gas at $T_s = 130\,°C$ are shown: all H_3^+ ions that bombard the grounded electrode have energies between 20 and 40 eV and thus contribute to the chemical sputtering. With the Monte Carlo code (see supplementary material Section 2), we found that the position of the peak in the H_3^+ IED at the powered electrode (E_P) can be calculated with the measured V_{DC} and the plasma potential (V_{pl})

$$E_P[\mathrm{eV/ion}] = 0.98(|V_{DC}| + V_{pl}). \quad (3)$$

The experimental V_{pl} for a given P_{rf} is roughly equal to the H_3^+ IED peak position at the grounded electrode. The inset table of Fig. 3 shows the experimental V_{pl}, V_{DC}, E_P, and V_{rf}. When we put the experimental values in Eq. (3), we find E_P at 34, 53, and 72 eV for $P_{rf} = 57$, 114, and 171 mW cm^{-2}, respectively.

With the equations and assumptions presented above, we calculated the etch yields Y_G and Y_P of the P_{rf} series (see Table II). The starting point is the discharge at $P_{rf} = 57$ mW cm^{-2}, where RGA measurements showed that chemical sputtering introduces a flow of Si atoms into the discharge that is equivalent to 0.35 sccm SiH_4 (see Section IV D). With an inlet flow of 0.35 sccm SiH_4, the fluid model computed $r_{gross,G} = 133$ nm/h and the tabulated $\Gamma_{G,Hy+}$ and $\Gamma_{P,Hy+}$ fluxes at $P_{rf} = 57$ mW cm^{-2}. With the net deposition rate, $r_{net,G}$, of Table I, using Eq. (2b), the etch rate becomes: $r_{etch,G} = 163$ nm/h. This value is used to calculate Y_G with Eq. (2a): $Y_G = 0.3$. Y_P is then the only unknown left in Eq. (1): $Y_P = 0.40$. Now Y_G is kept fixed at 0.3 in the Y_P computations for $P_{rf} = 114$ and 171 mW cm^{-2}. By using the measured $r_{net,G}$ and $Y_G = 0.3$, we obtained the gross deposition rate and found a higher value than obtained for 0.35 sccm SiH_4, showing that chemical sputtering at higher P_{rf} created a larger equivalent SiH_4 inflow (i.e., Si_{inlet} in Eq. (1)). The fluid model was therefore rerun with an inflow of 1 sccm SiH_4 and 60 sccm H_2 to compensate for possible changes in the ion fluxes, resulting in the tabulated values. Since H_y^+ ion energies at the grounded electrode at $P_{rf} = 171$ mW cm^{-2} are comparable to the ion energies at $P_{rf} = 57$ mW cm^{-2} at the powered electrode, we also made a calculation for the situation with $Y_G = 0.4$ at $P_{rf} = 171$ mW cm^{-2} (last row of Table II). This resulted in $Y_P = 0.65$ at $P_{rf} = 171$ mW cm^{-2}, which is slightly higher than at $P_{rf} = 114$ mW cm^{-2}. It is expected that the chemical sputtering yield increases with higher H_y^+ ion energies for the range of energies investigated and therefore with increasing P_{rf} (see supplementary material Section 1 for the complete computation of the chemical sputtering yields).

The chemical sputtering yield is not expected to vary with the H_y^+ flux, since $\Gamma_{G,Hy+}$ and $\Gamma_{P,Hy+}$ stay well below 10^{20} ions m^{-2} s^{-1} in the etch experiments (see Table II). Roth[15] observed that for chemical sputtering of graphite by H_y^+ fluxes above 10^{21} ions m^{-2} s^{-1}, the yield is decreasing, possibly related to a less efficient H passivation of dangling carbon bonds. Table II shows that the computed $\Gamma_{G,Hy+}$ increases by a factor 1.9, but $\Gamma_{P,Hy+}$ increases by a factor 2.7 at the powered electrode when increasing P_{rf} from 57 to 171 mW cm^{-2}. Thus, increased etching at the powered electrode at higher P_{rf} results in a higher $r_{net,G}$. This trend cannot be the result of atomic H etching alone, since $G_{a,flux}$ is slightly higher than $P_{a,flux}$ (see Table II). The powered electrode is not heated and is therefore significantly cooler than the grounded electrode at $T_s = 130\,°C$. When the substrate was cooled down to room temperature, we observed the same trend: an increasing $r_{net,G}$ with increasing P_{rf} (last column of Table II). Moreover, $r_{net,G}$ at $T_s = 25\,°C$ is of the same order of magnitude as at $T_s = 130\,°C$, as is expected in the case of chemical sputtering.

TABLE II. Modeling results at $p = 25$ Pa and $T_s = 130\,°C$.

P_{rf} (mW cm^{-2})	$\Gamma_{G,Hy+}$ (m^{-2} s^{-1})	$\Gamma_{P,Hy+}$ (m^{-2} s^{-1})	SiH_4 (sccm)[a]	Y_G	Y_P	$r_{gross,G}$ (nm/h)	$r_{etch,G}$ (nm/h)	$r_{net,G}$ (nm/h)	$G_{a,flux}$ (m^{-2} s^{-1})	$P_{a,flux}$ (m^{-2} s^{-1})
57	0.8×10^{19}	1.3×10^{19}	0.35	0.3	0.40	133	163	−30	1.1×10^{20}	1.0×10^{20}
114	1.2×10^{19}	2.5×10^{19}	0.83	0.3	0.60	351	256	+95	1.7×10^{20}	1.6×10^{20}
171	1.4×10^{19}	3.3×10^{19}	0.99	0.3	0.55	437	300	+137	2.1×10^{20}	1.9×10^{20}
171	1.4×10^{19}	3.3×10^{19}	1.21	0.4	0.65	537	400	+137	2.1×10^{20}	1.9×10^{20}

[a]Inflow of SiH_4 due to etching. The inflow of H_2 is kept at 60 sccm for all P_{rf} applied.

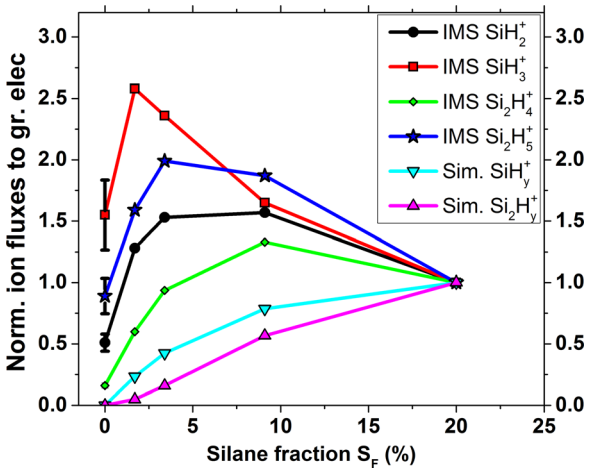

FIG. 4. Normalized measured IMS fluxes on the grounded electrode for SiH_2^+, SiH_3^+, $Si_2H_4^+$, and $Si_2H_5^+$ and simulated (Sim.) SiH_y^+ and $Si_2H_y^+$ ion fluxes. Fluxes are normalized to their values at $S_F = 20\%$.

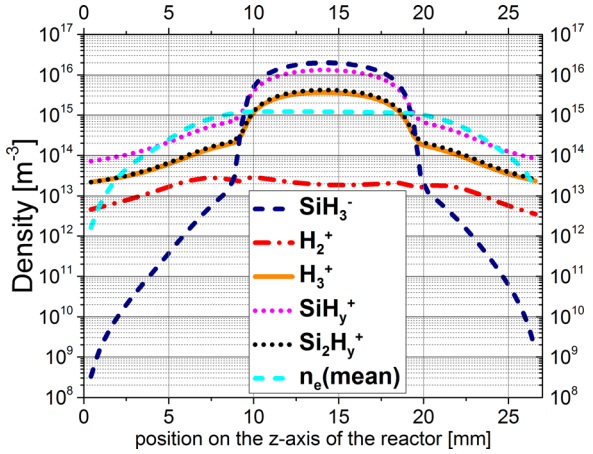

FIG. 5. Modeled time averaged electron density n_e and ion densities of SiH_3^-, H_2^+, H_3^+, SiH_y^+, $Si_2H_y^+$ on the z-axis of the reactor ($z = 0$ is the plane of the powered electrode and $z = 27$ mm the plane of the grounded electrode) at $S_F = 20\%$ as simulated by the fluid model. This discharge has a $V_{DC} = -29$ V and $V_{rf} = 81$ V at $P_{rf} = 57$ mW cm^{-2}.

B. Ion fluxes in the S_F series

In Fig. 4, we show the simulated and measured $Si_xH_y^+$ fluxes towards the grounded electrode in our S_F series at $P_{rf} = 57$ mW cm^{-2}. The experimental $Si_xH_y^+$ fluxes are not proportional to S_F, whereas the fluid model computes an increasing $Si_xH_y^+$ flux with increasing S_F. The modelling results do not yet take chemical sputtering into account. The experimental fluxes displayed in Fig. 4 are computed by determining the area under the IEDs and normalizing the values with the area at $S_F = 20\%$. The measured SiH_y^+ and $Si_2H_y^+$ fluxes are initially increasing with S_F up to $S_F = 1.7\%$ or 3.4% and subsequently come down to the normalization point at $S_F = 20\%$. The measured SiH_y^+ IEDs consist predominantly of SiH_3^+: the SiH_3^+ flux is 3 times larger than the SiH_2^+ flux at $S_F = 20\%$. The normalized SiH_3^+ flux has a maximum at low S_F. This might be attributed[32] to a reaction that creates SiH_3^+: $H_3^+ + SiH_4 \rightarrow SiH_3^+ + 2H_2$. The central H_3^+ density is, namely, higher at $S_F = 1.7\%$ than at $S_F = 20\%$ and the central H_3^+ density is higher than the electron density (shown in Figs. 5 and 6). Also, the rate constant of this reaction is about one order higher in these discharges than the electron ionization rate constant for SiH_3^+ formation. Therefore, this reaction can create a SiH_3^+ flux that is not proportional to the silane fraction. This reaction and mechanisms that can be responsible for a higher SiH_3^+ flux than SiH_2^+ flux are further discussed in Section V B. $Si_2H_4^+$ and $Si_2H_5^+$ ions are formed by the electron ionization of Si_2H_6 or by one of the following three reactions: (1) $SiH_2^+ + SiH_4 \rightarrow Si_2H_4^+ + H_2$, (2) $SiH_2^+ + Si_2H_6 \rightarrow Si_2H_5^+ + SiH_3$, and (3) $SiH_3^+ + Si_2H_6 \rightarrow Si_2H_5^+ + SiH_4$.[32] There is some fluctuation in the $Si_xH_y^+$ fluxes at $S_F = 0\%$ and this is depicted with an error bar.

Drift to the electrodes is one of the mechanisms for a positive ion species ($Si_xH_y^+$ and H_y^+) to disappear from the discharge. The density of an ionic species in the bulk is determined by its production and loss rate. The ion fluxes are also determined by the central positive ion density, which is sustained by the negative charge in the plasma bulk. In the electronegative SiH_4-H_2 discharge, the negative charge is composed of electrons and SiH_3^- ions. SiH_3^- ions are formed in the dissociative attachment reaction

$$SiH_4 + e^- \rightarrow SiH_3^- + H. \quad (4)$$

Even at a low silane inflow, a considerable density of negative ions builds up at the discharge center. The negative charges are compensated by an equal amount of positive ions ($Si_xH_y^+$ and H_y^+) to ensure quasi-neutrality. Since the central negative charge density is predominantly built up by negative ions, these plasmas are called ion–ion plasmas. In an ion-ion plasma, the so-called ambipolar electric field is low, reducing the ion drift velocity. At $S_F = 1.7\%$, the central SiH_3^- density is lower and more confined to the middle of the discharge than at $S_F = 20\%$. To a lesser extent, the same is observed for the electron densities at $S_F = 1.7\%$ and 20%. The simulated ion and electron density distributions on the z-axis ($r = 0$) of the reactor are displayed at $S_F = 20\%$ in Fig. 5 and at $S_F = 1.7\%$ in Fig. 6.

At $S_F = 20\%$, the simulated SiH_y^+ production rate and flux are roughly 4.5 times higher than at $S_F = 1.7\%$, whereas the central SiH_y^+ density at $S_F = 20\%$ is 16 times higher than at $S_F = 1.7\%$. On the other hand, the H_3^+ central density at $S_F = 1.7\%$ (59 sccm H_2) is 1.7 times higher than at $S_F = 20\%$ (50 sccm H_2). The H_3^+ flux to the electrodes is 4 times higher at $S_F = 1.7\%$ than at $S_F = 20\%$ and this is equal to the increase in the H_3^+ production rate. At $S_F = 20\%$, the ambipolar electric field is lower than at $S_F = 1.7\%$: the H_3^+ density compensates the high SiH_3^- density to maintain charge neutrality and therefore the H_3^+ ion does not readily leave the plasma bulk. The H_2^+ central density is significantly smaller than the H_3^+ central density: H_2^+ reacts to H_3^+. Fig. 7 shows that simulated and measured H_2^+ and H_3^+ fluxes are decreasing considerably with increasing S_F and the flux fall with increasing S_F is steeper for H_3^+ than H_2^+. Fig. 7 also shows that the measured decrease in H_3^+ flux at the grounded electrode is much steeper than in simulations.

The simulated atomic H fluxes ($G_{a,flux}$ and $P_{a,flux}$) increase with increasing S_F: $G_{a,flux}$ increases from 1.15×10^{20} m^{-2} s^{-1}

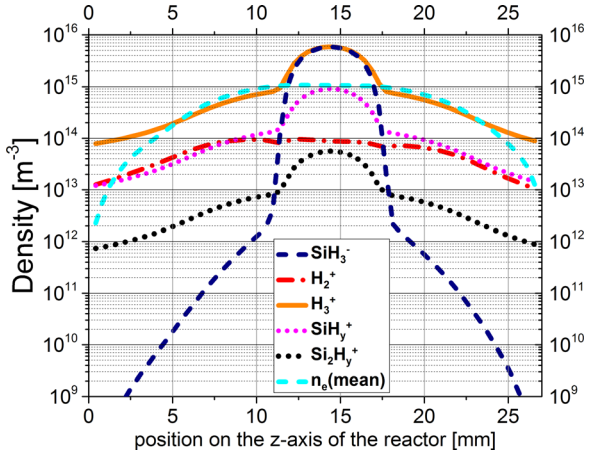

FIG. 6. Modeled time averaged electron density n_e and ion densities of SiH_3^-, H_2^+, H_3^+, SiH_y^+, $Si_2H_y^+$ on the z-axis of the reactor at $S_F = 1.7\%$ as simulated by the fluid model. This discharge has a $V_{DC} = -28$ V and $V_{rf} = 82$ V at $P_{rf} = 57$ mW cm^{-2}.

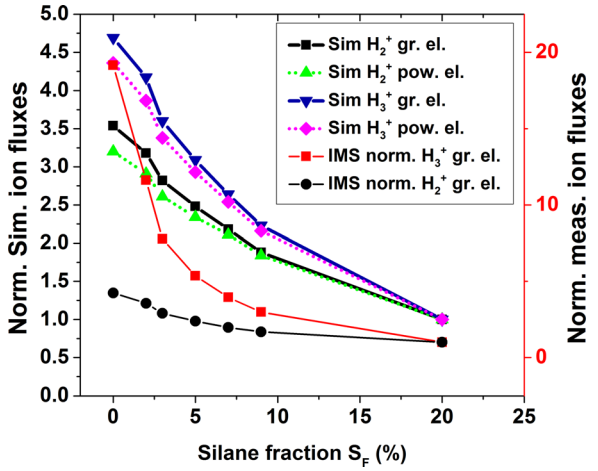

FIG. 7. Simulated (Sim) H_2^+ and H_3^+ fluxes to the grounded and powered electrodes normalized to their values at $S_F = 20\%$. Measured (IMS) H_2^+ and H_3^+ fluxes to the grounded electrode (right-hand y scale) normalized to their value at $S_F = 20\%$.

to 1.30×10^{20} m^{-2} s^{-1} for $S_F = 1.7\%$ to 20%. $P_{a,flux}$ is slightly lower than $G_{a,flux}$ for all S_F (e.g., $P_{a,flux}$ is 1.24×10^{20} m^{-2} s^{-1} at $S_F = 20\%$). The atomic H production rate due to H_2 dissociation is almost halved when S_F increases from 1.7% to 20%. However, the electron density is more confined to the middle of the discharge at low S_F and more H is formed by SiH_4 dissociation (e.g., reaction 4) at higher S_F and therefore the H flux increases slightly with S_F.

C. Effect of chemical sputtering on the $Si_xH_y^+$ flux trend in the S_F series

In Fig. 4, we observed that the experimental $Si_xH_y^+$ flux is not proportional to S_F but decreased with increasing S_F. Here, we test if this $Si_xH_y^+$ flux trend can be explained with the chemical sputtering model. In simulations and measurements of the S_F series, we see that the peaks of the H_3^+ IEDs on both electrodes (see supplementary material Section 2 A, Figs. S2–S4) are well above the threshold energy ($E_{dam} = 20$ eV) for damage creation in c-Si[22] by H_y^+ ions and therefore chemical sputtering is expected to occur on both electrodes. The measured H_3^+ peak position at the grounded electrode is around 28 ± 1 eV for all S_F, and with Eq. (3) we determined the experimental H_3^+ bombarding energy on the powered electrode to be 36 ± 1 eV ($V_{DC,meas} = -7 \pm 1$ V and $V_{pl,meas} = 30 \pm 0.5$ V) for all S_F.

Now we include the contribution of chemical sputtering by H_y^+ ions on both electrodes to the modeled SiH_y^+ flux in the S_F series (see Fig. 8). The sum of the SiH_y^+ flux created from the SiH_4 feedstock gas (SiH_y^+) and the SiH_y^+ flux as a result of H_y^+ chemical sputtering is labelled SiH_y^+ (corr). We modeled a discharge of 0.35 sccm SiH_4 and 60 sccm H_2 to determine the SiH_y^+ flux created with a pure H_2 inlet flow. The amount of SiH_4 created in the chemical sputtering process is proportional to the sum of the H_y^+ fluxes to the electrodes. Therefore, the amount of SiH_y^+ added by the correction at higher S_F is a fraction of the SiH_y^+ in the discharge with 0.35 sccm SiH_4 and this is visible in Fig. 8.

The SiH_y^+ (corr) flux trend in Fig. 8 is slightly closer to the experimental SiH_y^+ trend (see Fig. 4). There is, however, still a significant difference between the simulated and measured $Si_xH_y^+$ flux trend and therefore we explore other mechanisms in Section V B. Chemical sputtering in the S_F series does not significantly affect the deposition rate for $S_F > 1.7\%$. For $S_F \leq 1.7\%$, the deposition rate calculated by the fluid model is still close to the experimental value (see Fig. 9).

D. SiH_4 depletion fractions in the S_F series

From the SiH_2^+ RGA signal (see Fig. 10), we derived that at $S_F = 0\%$ and $P_{rf} = 57$ mW cm^{-2}, an amount equal to 0.35 sccm SiH_4 is added to the 60 sccm H_2 inlet flow. (This result is used in Section IV A.) To obtain this value, we assumed that the depletion fraction F_D in this discharge is the same as for $S_F = 1.7\%$ (i.e., 1 sccm SiH_4), being $F_D = 0.39 \pm 0.02$. F_D is determined experimentally: F_D is the ratio of the loss in SiH_2^+ RGA signal as a consequence of switching on the plasma to the SiH_2^+ RGA signal without

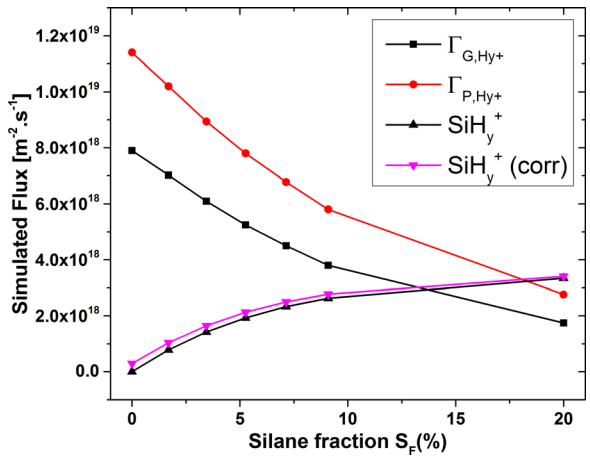

FIG. 8. This graph shows the following modeled fluxes: the SiH_y^+ flux to the grounded electrode (SiH_y^+) as modeled without chemical sputtering, the H_y^+ ion flux to the grounded ($\Gamma_{G,Hy+}$) and powered ($\Gamma_{P,Hy+}$) electrode, and the result of the correction of the SiH_y^+ flux to the grounded electrode with the chemical sputtering model (SiH_y^+ (corr)).

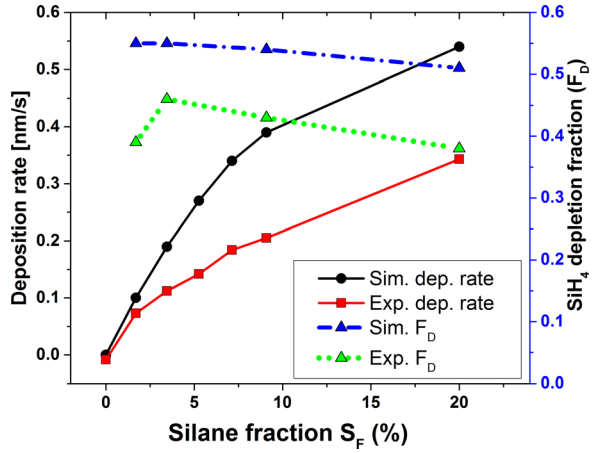

FIG. 9. Deposition rate and depletion fraction versus the silane fraction in the feedstock gas.

the plasma (i.e., in the presence of the gas mixture). F_D is the fraction of SiH_4 feedstock that is consumed in plasma reactions, and the remaining fraction is pumped away. In our simulations of the S_F series, the residence time of the neutrals is 0.17 s for a total gas inlet flow of 60 sccm at 25 Pa.

F_D is decreasing from $F_D = 0.45 \pm 0.01$ to 0.38 ± 0.02 for $S_F = 3.4\%$ to 20% (see Fig. 9). At higher S_F, a lower percentage of the SiH_4 feedstock is consumed due to a lower electron temperature. At higher S_F, also more $Si_{x>1}H_y$ molecules and radicals are formed, which are eventually pumped away. Therefore, the increase in the simulated deposition rate levels off for S_F above 5%. On the other hand, F_D at $S_F = 1.7\%$ is lower than at $S_F = 3.4\%$ since enhanced etching at low S_F brings more SiH_4 back into the discharge and therefore it looks as if less SiH_4 is consumed. At $S_F = 0\%$, a clear Si* OES signal is measured (see supplementary material Section 3 C, Fig. S7), which is formed by chemically sputtered SiH_4. Fig. 10 shows that the SiH_2^+ and $Si_2H_4^+$ RGA signals that were measured with the plasma switched on are proportional to S_F, leading to an almost constant F_D. At $S_F = 0\%$, the signal clearly deviates from this proportionality to the SiH_4 inlet flow (i.e., 0 sccm SiH_4) and this is the result of chemical sputtering.

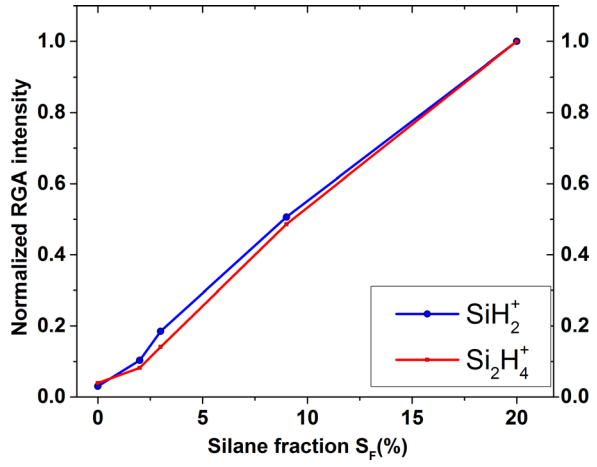

FIG. 10. The normalized SiH_2^+ and $Si_2H_4^+$ RGA signals with the plasma on of the S_F series. The signal intensities are normalized to their values at $S_F = 20\%$.

E. Control experiments and simulations

With a number of control experiments and simulations, we exclude some other mechanisms that can be considered responsible for the discrepancy between the simulated and experimental $Si_xH_y^+$ flux trend in the S_F series. In particular, we address the possibility of physical sputtering and the difference between the simulated and measured V_{DC} and V_{rf} voltages.

1. Absence of physical sputtering

In this control experiment, we made IMS measurements of an Ar-SiH_4 dilution series. Here, the SiH_3^+ flux was proportional to the SiH_4 concentration in the Ar-SiH_4 feedstock gas mixture (see supplementary material Section 3 D, Fig. S8). When we applied a pure Ar plasma (60 sccm Ar, $p = 25$ Pa, $P_{rf} = 57$ mW cm^{-2}) in a reactor with a Si layer on the powered electrode, we did not detect a SiH_3^+ signal during IMS measurements. This confirms that for the plasma conditions used, the Ar ion energies are below the threshold energy for physical sputtering. However, as soon as we added a small amount of H_2 gas to the feedstock gas mixture, a significant SiH_3^+ signal was observed due to chemical sputtering.

2. The effect of an externally applied bias

In Section IV B, we showed experimental and simulated H_3^+ and SiH_y^+ flux trends and their density profiles. The ion-ion plasmas of the S_F series are rigid in the sheath and bulk in the sense that the ion density distributions resist deformation by the rf electric field and an externally applied dc voltage that is added to V_{DC}. The sheath is formed by an almost immobile ion density profile and an oscillating electron density profile, whereas the bulk ion–ion plasma only reacts to the average electric field. In Fig. 11, the broadness and central alignment of the average potential profile and SiH_3^- ion density at $S_F = 1.7\%$ and 20% are compared. At low S_F, the n_e and SiH_3^- density are more confined to the middle of the reactor and this results in a narrower plateau of the potential profile. The dc self-bias shifts the n_e and SiH_3^- density slightly towards the grounded electrode ($z = 27$ mm). The sheath at the powered electrode is about 2 mm wider than at the grounded electrode.

We investigated the changes when the simulated V_{DC} is pinned at the experimentally determined $V_{DC} = -7$ V by an externally applied bias for $S_F = 1.7\%$ and 20% (see Fig. 11). The discharge becomes more symmetric and the plasma potential increases with about 7 ± 1 V. The externally applied bias voltage introduces a small DC current through the discharge that affects the ion fluxes only a little bit. Therefore, it can be concluded that the ion fluxes from the simulated discharge ($V_{DC} = -29$ V and $V_{rf} = 81$ V at $S_F = 20\%$) represent the ion fluxes of the experimental discharge ($V_{DC} = -7$ V and $V_{rf} = 62$ V at $S_F = 20\%$) in spite of the different V_{DC} and V_{rf}. This phenomenon is also experimentally observed in Fig. S6 of the supplementary material, which shows the effect of an externally applied bias of +69 V on the SiH_3^+ IEDs of the S_F series.

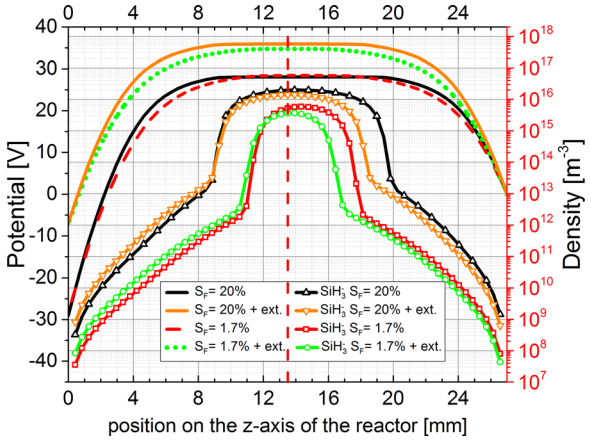

FIG. 11. Simulated average potential profiles (y-axis on the left side) and SiH_3^- ion density (open symbols and y-axis on the right side) profiles at $S_F = 20\%$ and $S_F = 1.7\%$ for the same discharges as depicted in Figs. 5 and 6, respectively. The potential and SiH_3^- ion density profiles are also shown with an externally applied V_{DC} (denoted + ext. in the legend) that pins the resultant V_{DC} at −7 V.

V. DISCUSSION

A. Chemical sputtering

In the chemical sputtering process, a collision cascade of a H_y^+ ion inside the Si layer creates strained or broken Si–Si bonds. Strained bonds are readily broken and Si dangling bonds are passivated by the ubiquitous atomic H in the growth zone that is supplied by the plasma. This mechanism forms loosely bound reaction products that are thermally desorbed. Thus, in the chemical sputtering process, the H_y^+ ions enhance the atomic H etching process.

The H_y^+ flux in our experiments consists of 90% H_3^+ ions and the rest is H_2^+ (the amount of H^+ is negligible). Mitchell *et al.*[11] found that the thermalized H_3^+ ion is converted into 3 H or H_2 + H at the moment of impact due to dissociative recombination.[11,26,33] In this way, the H_3^+ ion brings not only energy to break the Si-Si bond (2.3 eV) but also atomic H to passivate the Si dangling bonds and to form a stable desorption product. The formation of the Si-H bond releases a few eV as thermal energy[9] (the amount of energy depends on the Si-H bond configuration) and this is usually more than the SiH_4 desorption energy:[34] $E_{des} = 1.8 \pm 0.1$ eV. The desorption product is Si_xH_{2x+2}.

The H_y^+ ions bombarding the two electrodes in the P_{rf} series (Section IV A) have energies well above $E_{dam} = 20$ eV. In our chemical sputtering model, we assumed that the etch yield increases with the H_y^+ bombardment energy and found $Y_G = (0.3–0.4) \pm 0.1$ and $Y_P = (0.4 \pm 0.66) \pm 0.1$ for P_{rf} from 57 to 171 mW cm^{-2}. In studies with carbon targets, chemical sputtering of carbon by impinging H_y^+ ions in an extreme ultraviolet (EUV) induced H_2 plasma and a microwave (surface wave discharge) H_2 plasma at low pressure and low bias voltage[35] with a yield of 0.5 C atom per impinging H_y^+ ion has been reported. It is also similar to the 0.6 C atom per impinging Ar^+ ion reported by Hopf *et al.*[36] achieved with a 20 eV Ar^+ beam in combination with an abundant supply of atomic hydrogen.[36] The yields we found for silicon are of the same order as these values for chemical sputtering of carbon.

A study by Balden and Roth[16] on c-Si etching with monoenergetic D_3^+ ion beams for T_s ranging from 25 °C to 827 °C revealed that the etch yield for c-Si by a 20 eV D_3^+ beam has a pronounced maximum around 130 °C, being 0.015 Si atom per impinging D_3^+ ion. This temperature maximum in the yield has not been reported for atomic H produced with a tungsten filament.[13] Since the Si etch yield of the 20 eV D_3^+ beam is much lower than one should expect from chemical sputtering, Balden and Roth suggested that E_{dam} is about 30 eV for c-Si. Then, the results confirm that etching of D_3^+ with ion energies below E_{dam} is similar to atomic H etching: the etch yield of atomic H etching[6,7] at 130 °C is about 0.015. It should be noted that the atomic H etch yield is more than two orders of magnitude lower than the chemical sputtering etch yield, and the H_y^+ fluxes are only one order of magnitude lower than the atomic H fluxes in the P_{rf} and S_F series presented.

The relative substrate temperature independence of the chemical sputtering mechanism reported by Balden and Roth[16] and Roth[15] for chemical sputtering of hydrogenated carbon matches our experimental results. In our P_{rf} series (Section IV A), the net deposition rate is only reduced by 26% when the substrate temperature is lowered from 130 °C to room temperature at $P_{rf} = 114$ mW cm^{-2}. Moreover, the plasma heats the substrate only a few °C and therefore this effect is neglected in the analysis.

A model for H_y^+ chemical sputtering during Si deposition by a SiH_4-H_2 cc PECVD discharge has not been presented before, but the mechanism has been used before. Vepřek and Mareček[37] report chemical transport by chemical sputtering of c-Si by a PECVD H_2 plasma at 13 Pa which results in a deposition rate in the order of 10 nm/h on a heated glass substrate. The atmospheric-pressure plasma enhanced chemical transport (APECT) method described by Ohmi *et al.*[38] applies chemical sputtering. This method uses an H_2–He cc PECVD discharge at atmospheric pressure to deposit a poly-crystalline Si film by chemical sputtering, but they do not report the ion energies or species involved. Otobe *et al.*[14] report an a-Si:H etch rate in the order of 200 nm/h for etching with a H_2 PECVD discharge at $T_s = 150$ °C, $P_{rf} = 180$ mW cm^{-2}, and $p = 27$ Pa. The etch rate for c-Si etching is a factor 10 lower under the same plasma conditions. An etch rate of 200 nm/h matches the etch rates we found in the P_{rf} series (see $r_{etch,G}$ in Table II) with similar plasma parameters.

B. Ion flux trends in the S_F series

The measured SiH_2^+, SiH_3^+, $Si_2H_4^+$, and SiH_5^+ fluxes in our S_F series decreased for $S_F = 3.4\%–20\%$. This trend is in good agreement with the $Si_xH_y^+$ flux trends observed by Horvath and Gallagher[39] in their S_F series, but this trend is not reproduced by our fluid model (see Fig. 4). H_y^+ chemical sputtering of Si brings Si_xH_{2x+2} neutrals into the discharge at low S_F as we learned from the RGA signals in Fig. 10 and the Si* OES signal (Fig. S7) at $S_F = 0\%$ and can partly explain the measured $Si_xH_y^+$ flux trends (see Fig. 8). Changes in the plasma parameters of the S_F series as a cause of the decreasing $Si_xH_y^+$ flux must be excluded. Although the rate constant for ionization decreases from $S_F = 1.7\%$ to 20%, it is too little (62% in the electron temperature range of interest) to

compensate for the decrease in SiH_4 density due to the lower S_F. In addition, the central n_e increases slightly and is less confined to the middle of the discharge when S_F increases from 1.7% to 20%.

The high SiH_3^+-to-SiH_2^+-flux-ratios measured might provide a clue for the enhanced $Si_xH_y^+$ flux at low S_F. We observe a decreasing SiH_3^+-to-SiH_2^+-flux-ratio from 7 to 3 for $S_F = 1.7\%$ to 20%. The ratio of the ionization cross sections for SiH_3^+ and SiH_2^+ formation is 0.72 at an electron energy of 15 eV.[40] The latter ratio is only gradually increasing up to 0.83 at 70 eV electron energy and therefore does not strongly depend on S_F. Thus, we considered other reaction mechanisms. First, Turban *et al.*[41] and Perrin *et al.*[32] show that it is likely that a SiH_y^+ ion picks up an H atom in a reaction with SiH_4 in the bulk, for example, with reaction 5 below. Second, one could suggest that SiH_2^+ recombines more easily with SiH_3^- in the plasma bulk than SiH_3^+, but actually the opposite is true: Reents and Mandich[42] found out that the SiH_3^+ mobility in pure silane plasmas is 3.5 times lower than the SiH_2^+ mobility. The low mobility of SiH_3^+ at high S_F increases its density in the plasma bulk and reduces its flux. Third, the endothermic reaction of SiH_y^+ with D_2 reported by Allen *et al.*[43] can be considered. Thus, SiH_2^+ that collides in the sheath with H_2 can create SiH_3^+. However, the mean free path of this reaction is 40 mm at 25 Pa and therefore unlikely to occur. Finally, Allen *et al.*[43] and Perrin *et al.*[32] mention reactions 6 and 7

$$SiH_2^+ + SiH_4 \rightarrow SiH_3^+ + SiH_3, \quad (5)$$

$$H_3^+ + SiH_4 \rightarrow SiH_3^+ + 2H_2, \quad (6)$$

$$H_2^+ + SiH_4 \rightarrow SiH_3^+ + H_2 + H. \quad (7)$$

At low S_F, especially reaction 6 becomes dominant. To simulate the effect of reactions 5–7, the SiH_2^+ and SiH_3^+ ions were treated as separate species in the fluid model. This resulted in a higher SiH_y^+ flux and the maximum in the SiH_y^+ flux shifted to a lower S_F (compare SiH_y^+(G,ls) and SiH_y^+(G,ss) in Fig. 12). We found a 100% increase of the SiH_y^+ flux at $S_F = 1.7\%$ and a 25% increase at $S_F = 20\%$. The new SiH_y^+(G,ss) flux contributed about 30% to the a-Si:H growth rate at $S_F = 1.7\%$. The simulated SiH_3^+-to-SiH_2^+-flux-ratio ranged from 3.1 to 4.2 for $S_F = 1.7\%$ to 20%. We also observed that the decrease in the normalized H_3^+ flux with increasing S_F became much steeper and therefore more in agreement with the measured trend (see Fig. 7). The Si created by the chemical sputtering process was not added to the SiH_4 inlet flow in the simulations of Fig. 12. With this addition, the maximum in the $Si_xH_y^+$ flux trend will shift slightly to a lower S_F, but there is still a significant difference between the measured and simulated $Si_xH_y^+$ flux trend at low S_F. A sensitivity study of the rate constants of reactions 5–7 is recommended for further analysis.

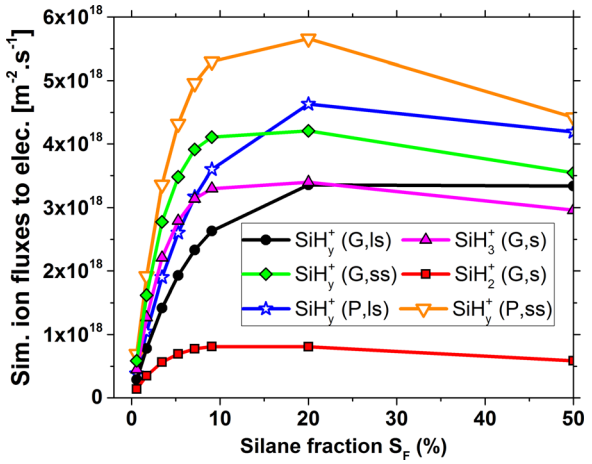

FIG. 12. Simulated SiH_y^+ ion fluxes to the grounded (G) and powered (P) electrodes. SiH_y^+(G,ls) (also shown in Fig. 4) is the flux of the SiH_y^+ lump sum (ls) calculation, SiH_3^+ (G,s) and SiH_2^+(G,s) are fluxes of the split (s) computation and the split fluxes summed (ss) gives SiH_y^+(G,ss) (i.e., SiH_3^+(G,s) plus SiH_2^+ (G,s)). Also the SiH_y^+ ion fluxes to the powered electrode are shown: the SiH_y^+(P, ls) lump sum and the sum of SiH_2^+(P,s) and SiH_3^+(P,s), being SiH_y^+(P,ss).

VI. CONCLUSIONS

We observed that the experimental $Si_xH_y^+$ flux is not proportional to S_F for SiH_4-H_2 discharges with silane fractions ranging from $S_F = 0\%$ to 20%. In addition, we experimentally observed that the H_3^+ flux decreases more than eleven times from $S_F = 1.7\%$ to 20%. This brought us to the hypothesis of Si etching by chemical sputtering with H_y^+ ions. This etching mechanism has a rate proportional to the H_y^+ ion flux and therefore brings more Si into the discharge at low S_F.

We found chemical sputtering of silicon films by H_y^+ ions in an asymmetric VHF PECVD discharge. A P_{rf} series of discharges with pure H_2 inlet flow resulted in chemical transport of Si from the powered electrode to the substrate. Modelling showed that in this P_{rf} series the flux of H_y^+ ions to the powered electrode was larger than to the grounded electrode, whereas the atomic H flux to the powered electrode was smaller than to the grounded electrode. Moreover, a control experiment (supplementary material Section 3 A) showed that the major part of the SiH_y^+ signal during IMS measurements is formed by Si etched from the powered electrode. With our chemical sputtering model, we determined an etch yield (Si atoms etched per bombarding H_y^+ ion) at the grounded electrode of $Y_G = (0.3\text{–}0.4) \pm 0.1$ and at the powered electrode the etch yield varied from $Y_P = (0.4$ to $0.65) \pm 0.1$ for $P_{rf} = 57\text{–}171$ mW cm^{-2}. These yields are of the same order of magnitude as yield values reported in the literature for chemical sputtering of hydrogenated carbon by H_y^+ ions.

With mass resolved ion bombardment measurements and numerical modeling, we gained a good understanding of the ion densities, energies, and fluxes towards the electrodes in the S_F series. We observed that the H_y^+ bombardment energies at both electrodes are well above $E_{dam} = 20$ eV in our S_F series. The chemical sputtering mechanism, however, cannot completely explain the difference between the modeled and measured $Si_xH_y^+$ flux trends. Splitting the SiH_y^+ lump sum in the fluid model and the addition of the reaction between H_3^+ and SiH_4 that creates SiH_3^+ made the difference at low S_F smaller.

In an asymmetric discharge, the deposition rate on the grounded electrode at low S_F can be significantly enhanced

by chemical sputtering of Si from the cathode. By tuning the H_y^+ ion bombardment fluxes and energies with discharge power and gas pressure, this process can be optimized. Starting a deposition with a pure H_2 plasma allows to create a thin μc-Si:H seed layer on an amorphous substrate, such as glass, by chemical transport. This seed layer can subsequently be used for high rate μc-Si layer growth with a reduced or absent incubation layer.[44] Knowledge of the chemical sputter mechanism of Si by H_y^+ ions can be an asset for industry that uses cc PECVD plasmas at low S_F (and even with only H_2 feedstock gas) to deposit a-Si:H, μc-Si:H or poly-crystalline Si.

SUPPLEMENTARY MATERIAL

See supplementary material file for Figs. S1–S8. The supplementary material consists of the following sections: (1) Complete computation of the chemical sputtering yield, (2) modeling SiH_3^+ IEDs with the Monte Carlo code in the S_F series, (3) extra control experiments, titled: (A) "Powered electrode with and without a Si layer," (B) "exclusion of etching by electrons," (C) "Si* OES signal in the S_F series," and (D) "absence of physical sputtering."

ACKNOWLEDGMENTS

This research is part of the FLASH Perspectief program, supported by the Dutch Technology Foundation STW, which is part of the Dutch Organization for Scientific Research (NWO). The authors thank P. Dingemans for technical assistance.

APPENDIX: LIST OF FREQUENTLY USED VARIABLES

Variable	Units	Description
$A_{G/P}$	m^2	Surface area of the substrate holder ($A_G = 227\,cm^2$)/powered electrode ($A_P = 194\,cm^2$)
E_p	eV/ion	Peak position of the H_3^+ IED at the powered electrode
$\Gamma_{G/P,Hy+}$	ions $m^{-2}\,s^{-1}$	H_y^+ ion flux to the substrate holder/powered electrode
H_y^+	n/a	Name for the group of H_3^+ plus H_2^+ ions (concentration of H^+ ions is negligible)
n_{Si}	$m^{-2}\,nm^{-1}$	Si atomic density of pure silicon ($n_{Si} = 5 \times 10^{19}\,m^{-2}\,nm^{-1}$)
P_{rf}	mW cm^{-2}	Coupled power density divided by the surface area of the powered electrode (A_P)
$r_{etch,G}$	nm/h	Gross Si etch rate from the substrate holder (i.e., on the surface area A_G)
$r_{gross,G}$	nm/h	Gross Si deposition rate on the substrate holder (i.e., on the surface area A_G)
$r_{net,G}$	nm/h	Net Si deposition rate on the substrate holder (i.e., on the surface area A_G)
$Si_{inlet,P}$	atoms s^{-1}	Gross flow of Si atoms from the powered electrode due to chemical sputtering
$Si_{inlet,G}$	atoms s^{-1}	Gross flow Si atoms from the substrate (holder) due to chemical sputtering
Si_{inlet}	atoms s^{-1}	Total flow of Si atoms brought into the discharge by chemical sputtering (1 sccm $SiH_4 = 4.48 \times 10^{17}$ Si atoms s^{-1})
$Y_{G/P}$	atoms/ion	Chemical sputtering etch yield: Si atoms etched per bombarding H_y^+ ion

[1]B. Kalache, A. I. Kosarev, R. Vanderhaghen, and P. R. i Cabarrocas, J. Appl. Phys. **93**, 1262 (2003).
[2]M. Koster and H. M. Urbassek, J. Appl. Phys. **90**, 689 (2001).
[3]E. A. Hamers, W. G. J. H. van Sark, J. Bezemer, H. Meiling, and W. van der Weg, J. Non-Cryst. Solids **226**, 205 (1998).
[4]A. H. M. Smets, W. M. M. Kessels, and M. C. M. van de Sanden, J. Appl. Phys. **102**, 73523 (2007).
[5]K. Landheer, W. J. Goedheer, I. Poulios, R. E. I. Schropp, and J. K. Rath, Phys. Status Solidi A **213**, 1680 (2016).
[6]O. Leroy, G. Gousset, L. L. Alves, J. Perrin, and J. Jolly, Plasma Sources Sci. Technol. **7**, 348 (1998).
[7]J. Abrefah and D. R. Olander, Surf. Sci. **209**, 291 (1989).
[8]K. Wittmaack, Phys. Rev. B **68**, 235211 (2003).
[9]G. Cerofolini, Mater. Sci. Eng., R **27**, 1 (2000).
[10]J. Roth and J. Bohdansky, Appl. Phys. Lett. **51**, 964 (1987).
[11]J. B. A. Mitchell, J. L. Forand, C. T. Ng, D. P. Levac, R. E. Mitchell, P. M. Mul, W. Claeys, A. Sen, and J. W. McGowan, Phys. Rev. Lett. **51**, 885 (1983).
[12]Y. S. Hiraoka, Jpn. J. Appl. Phys., Part 1 **41**, 784 (2002).
[13]H. N. Wanka and M. B. Schubert, J. Phys. D: Appl. Phys. **30**, L28 (1997).
[14]M. Otobe, M. Kimura, and S. Oda, Jpn. J. Appl. Phys., Part 1 **33**, 4442 (1994).
[15]J. Roth, J. Nucl. Mater. **266–269**, 51 (1999).
[16]M. Balden and J. Roth, J. Nucl. Mater. **279**, 351 (2000).
[17]K. Saitoh, M. Kondo, M. Fukawa, T. Nishimiya, A. Matsuda, W. Futako, and I. Shimizu, Appl. Phys. Lett. **71**, 3403 (1997).
[18]B. G. Heil, U. Czarnetzki, R. P. Brinkmann, and T. Mussenbrock, J. Phys. D: Appl. Phys. **41**, 165202 (2008).
[19]T. Lafleur, R. W. Boswell, and J. P. Booth, Appl. Phys. Lett. **100**, 194101 (2012).
[20]B. Bruneau, J. Wang, J.-C. Dornstetter, and E. V. Johnson, J. Appl. Phys. **115**, 84901 (2014).
[21]P. J. Hargis, K. E. Greenberg, P. A. Miller, J. B. Gerardo, J. R. Torczynski, M. E. Riley, G. A. Hebner, J. R. Roberts, J. K. Olthoff, J. R. Whetstone, R. J. Van Brunt, M. A. Sobolewski, H. M. Anderson, M. P. Splichal, J. L. Mock, P. Bletzinger, A. Garscadden, R. A. Gottscho, G. Selwyn, M. Dalvie, J. E. Heidenreich, J. W. Butterbaugh, M. L. Brake, M. L. Passow, J. Pender, A. Lujan, M. E. Elta, D. B. Graves, H. H. Sawin, M. J. Kushner, J. T. Verdeyen, R. Horwath, and T. R. Turner, Rev. Sci. Instrum. **65**, 140 (1994).
[22]K. Landheer, M. Kaiser, F. Tichelaar, I. Poulios, R. E. I. Schropp, and J. K. Rath, "Decoupling high surface recombination velocity and epitaxial growth for silicon passivation layers on crystalline silicon" (unpublished).
[23]K. Landheer, "Transmission optimization of an RFEA" (unpublished).
[24]A. Descoeudres, L. Barraud, R. Bartlome, G. Choong, S. De Wolf, F. Zicarelli, and C. Ballif, Appl. Phys. Lett. **97**, 183505 (2010).
[25]G. J. Nienhuis, W. J. Goedheer, E. A. G. Hamers, W. G. J. H. M. van Sark, and J. Bezemer, J. Appl. Phys. **82**, 2060 (1997).
[26]R. K. Janev, D. Reiter, and U. Samm, FZ Jülich, Report No. Jül-4105, 2004.
[27]T. Sato and T. Goto, Jpn. J. Appl. Phys., Part 1 **25**, 937 (1986).
[28]A. V. Phelps, J. Phys. Chem. Ref. Data **19**, 653 (1990).
[29]R. K. Janev, W. D. Langer, D. E. Post, and K. Evans, *Elementary Processes in Hydrogen-Helium Plasmas* (Springer, Berlin, Heidelberg, 1987).
[30]V. Vahedi and M. Surendra, Comput. Phys. Commun. **87**, 179 (1995).
[31]A. Manenschijn and W. J. Goedheer, J. Appl. Phys. **69**, 2923 (1991).
[32]J. Perrin, O. Leroy, and M. C. Bordage, Contrib. Plasma Phys. **36**, 3 (1996).
[33]H. Tawara, Y. Itikawa, H. Nishimura, and M. Yoshino, J. Phys. Chem. Ref. Data **19**, 617 (1990).
[34]P. Martín, J. F. Fernández, and C. R. Sánchez, Phys. Status Solidi A **182**, 255 (2000).
[35]D. I. Astakhov, W. J. Goedheer, C. J. Lee, V. V. Ivanov, V. M. Krivtsun, A. I. Zotovich, S. M. Zyryanov, D. V. Lopaev, and F. Bijkerk, Plasma Sources Sci. Technol. **24**, 55018 (2015).
[36]C. Hopf, A. von Keudell, and W. Jacob, J. Appl. Phys. **94**, 2373 (2003).
[37]S. Vepřek and V. Mareček, Solid-State Electron. **11**, 683 (1968).
[38]H. Ohmi, H. Kakiuchi, and K. Yasutake, J. Appl. Phys. **118**, 45301 (2015).
[39]P. Horvath and A. Gallagher, J. Appl. Phys. **105**, 13304 (2009).
[40]H. Chatham, D. Hils, R. Robertson, and A. Gallagher, J. Chem. Phys. **81**, 1770 (1984).
[41]G. Turban, Y. Catherine, and B. Grolleau, Thin Solid Films **67**, 309 (1980).
[42]W. D. Reents and M. L. Mandich, J. Chem. Phys. **93**, 3270 (1990).
[43]W. N. Allen, T. M. H. Cheng, and F. W. Lampe, J. Chem. Phys. **66**, 3371 (1977).
[44]A. Verkerk, J. K. Rath, and R. Schropp, Phys. Status Solidi A **207**, 530 (2010).